Bulletin of Mathematical Biology (2004) **66**, 1313–1344
doi:10.1016/j.bulm.2003.12.005

A Calcium-based Phantom Bursting Model for Pancreatic Islets

RICHARD BERTRAM*

Department of Mathematics and Kasha Laboratory of Biophysics,
Florida State University,
Tallahassee,
Florida 32306,
USA

E-mail: bertram@math.fsu.edu

ARTHUR SHERMAN

Laboratory of Biological Modeling,
National Institute of Diabetes and Digestive and Kidney Diseases,
National Institutes of Health,
Bethesda,
Maryland 20892,
USA

Insulin-secreting β-cells, located within the pancreatic islets of Langerhans, are excitable cells that produce regular bursts of action potentials when stimulated by glucose. This system has been the focus of mathematical investigation for two decades, spawning an array of mathematical models. Recently, a new class of models has been introduced called 'phantom bursters' [Bertram *et al.* (2000) *Biophys. J.* **79**, 2880–2892], which accounts for the wide range of burst frequencies exhibited by islets via the interaction of more than one slow process. Here, we describe one implementation of the phantom bursting mechanism in which intracellular Ca^{2+} controls the oscillations through both direct and indirect negative feedback pathways. We show how the model dynamics can be understood through an extension of the fast/slow analysis that is typically employed for bursting oscillations. From this perspective, the model makes use of multiple degrees of freedom to generate the full range of bursting oscillations exhibited by β-cells. The model also accounts for a wide range of experimental phenomena, including the ubiquitous triphasic response to the step elevation of glucose and responses to perturbations of internal Ca^{2+} stores. Although it is not presently a complete model of all β-cell properties, it demonstrates the design principles that we anticipate will underlie future progress in β-cell modeling.

*Author to whom correspondence should be addressed.

0092-8240/04/051313 + 32 $30.00/0

1. INTRODUCTION

Pancreatic β-cells are located in cell clusters within the pancreas called the islets of Langerhans. These micro-organs monitor the glucose concentration in the blood, and secrete the hormone insulin in response to elevated glucose levels. Since insulin is necessary for the uptake of glucose by other cells in the body, the proper functioning of β-cells is crucial for glucose homeostasis. Malfunctioning β-cells can lead to type II diabetes (Lang *et al*., 1981).

Both the average level and temporal pattern of insulin secretion are important for proper glucose homeostasis (Matthews *et al*., 1983). *In vitro* and *in vivo* data show that insulin secretion is oscillatory with period of several minutes (Chou and Ipp, 1990; Longo *et al*., 1991; O'Meara *et al*., 1993), and *in vitro* these oscillations have been shown to be in-phase with oscillations in the free cytosolic Ca^{2+} concentration (Bergsten *et al*., 1994; Bergsten, 1995). It has been established in both single β-cells and intact islets (Santos *et al*., 1991; Zhang *et al*., 2003) that these Ca^{2+} oscillations reflect a bursting pattern in the β-cell electrical activity. Electrical bursting, which consists of periodic active phases of cell firing followed by silent phases of hyperpolarization, was first detected *in vitro* in mouse islets by Dean and Mathews (1970) and has been confirmed *in vivo* (Sánchez-Andrés *et al*., 1995; Valdeolmillos *et al*., 1996).

One of the striking features of bursting in islets and isolated β-cells is the heterogeneity of periods, which range over two orders of magnitude, from a few seconds to a few minutes. We divide these oscillations into three classes. 'Fast bursting' has a period between 2 and 5 s. These oscillations are often observed in single cells (Kinard *et al*., 1999; Zhang *et al*., 2003) and in islets when the neurotransmitter acetylcholine is present (along with a stimulatory concentration of glucose) in the bath (Cook *et al*., 1981; Bertram *et al*., 1995; Bordin *et al*., 1995). 'Medium bursting' oscillations have a period ranging from 10 to 60 s. These are typically observed in islets with stimulatory glucose concentrations. 'Slow bursting' oscillations have a period ranging from 2 to 4 min and have been observed in both single cells (Ashcroft *et al*., 1984) and islets (Valdeolmillos *et al*., 1996; Liu *et al*., 1998). Medium bursting can be converted to slow bursting by application of epinephrine (Cook and Perara, 1982), or amino acids (Martín and Soria, 1995). Note that what we call 'medium bursting' is sometimes called 'fast bursting' by others.

Early mathematical models of β-cells were constructed to describe medium bursting, the type first and most often observed in islets. The first Hodgkin–Huxley type model for β-cells was developed by Chay and Keizer (1983). It was based on a hypothesis of Atwater and Rojas (Atwater *et al*., 1980) that slow negative feedback by cytosolic Ca^{2+} (c) acting on Ca^{2+}-activated K^+ (K(Ca)) channels drives bursting. However, subsequent Ca^{2+} imaging data seemed to indicate that c changes too rapidly to account for medium bursting (Santos *et al*., 1991). Later β-cell models differed largely in the slow process postulated to drive bursting. These included

voltage-dependent inactivation of a Ca^{2+} current (Keizer and Smolen, 1991), and oscillations in nucleotide concentrations (Keizer and Magnus, 1989; Smolen and Keizer, 1992).

The first models to explicitly address the variability of β-cell oscillations were proposed by Chay. The main mechanism for oscillations was variation in the Ca^{2+} concentration in the endoplasmic reticulum (ER), which directly or indirectly modulates one or more Ca^{2+}-dependent channels (Chay, 1996, 1997). Here we analyze in detail how the ER exerts its effects using our recently proposed phantom bursting model (PBM).

The PBM is a general paradigm for temporal plasticity in bursting in β-cells, in which bursting is driven by the interaction of two slow variables with disparate time constants (Bertram *et al*., 2000). The original implementation featured two generic slow variables, s_1 and s_2, with time constants of 1 s and 2 min, respectively. Depending on the conductance $g_{s,1}$ of the s_1 current, the PBM can produce bursting with periods ranging from a few seconds to a few minutes. When $g_{s,1}$ is large, the bursting that results is fast, driven entirely by s_1. When $g_{s,1}$ is small, s_1 has little influence, and the bursting that results is driven by s_2 and is slow. At intermediate conductance values both s_1 and s_2 contribute, yielding medium bursting. We call this latter case 'phantom bursting', since there is no single slow process with a time constant similar to the burst period; the bursting is a 'phantom' effect of the interaction of two slow variables with disparate time constants.

Phantom bursting is a dynamic concept and is not tied to a specific biophysical implementation. From a biological perspective, however, it is desirable to identify potential slow variables and to understand how these might interact to produce the range of bursting oscillations observed in β-cells. In this study, we show how three plausible slow processes can interact to drive bursting with the full range of periods exhibited by β-cells. These processes are the cytosolic Ca^{2+} concentration, the ER Ca^{2+} concentration, and the ADP/ATP ratio (ADP = adenosine diphosphate, ATP = adenosine triphosphate). We use the model to interpret the results of various *in vitro* experiments and identify data that are not yet reproduced by the model.

We begin with a description of a simple Chay–Keizer-like model with a single slow variable, the cytosolic Ca^{2+} concentration. Because Ca^{2+} changes only moderately slowly this model produces fast bursting and is limited to a small range of burst frequencies. We then add a second slow variable, the Ca^{2+} concentration in the ER, which varies more slowly than cytosolic Ca^{2+}. Using an extension of the fast/slow analysis pioneered by Rinzel (1985), we demonstrate how the two slow variables interact to produce fast, medium, or slow bursting. Finally, we use the model to interpret the conversion of medium to fast bursting that occurs in the presence of a muscarinic agonist.

The geometrical fast/slow analysis suggests an additional degree of freedom that can be utilized to increase further the richness of the bursting dynamics. We extend the model in this direction, introducing the ADP/ATP nucleotide ratio as a third

slow variable. This extension confers greater robustness on the model, especially for slow bursting. Additionally, the redundancy between the two slowest variables allows the model to account in large measure for data showing that slow bursting persists in the presence of an ER Ca^{2+} pump blocking agent (Liu *et al.*, 1995), even when most of the ATP-sensitive K^+ channels are blocked (Fridlyand *et al.*, 2003a). Finally, the presence of a slow ER and a slow nucleotide ratio allows the model to reproduce the characteristic triphasic response to a step increase in the external glucose concentration (Meissner and Atwater, 1976). The various models described in the text and their abilities to reproduce experimental observations are summarized in Table 4 in the Discussion section.

2. BURSTING WITH A SINGLE SLOW VARIABLE

2.1. ***The basic model.*** The basic model, which is essentially equivalent to the Chay–Keizer model (Chay and Keizer, 1983), consists of a Ca^{2+} current, I_{Ca}, a delayed rectifier K^+ current, I_K, a Ca^{2+}-dependent K^+ current, $I_{K(Ca)}$, and a nucleotide-sensitive K^+ current, $I_{K(ATP)}$. In the basic model, the ratio ADP/ATP is constant, so the conductance $g_{K(ATP)}$ is also constant. The differential equations for membrane potential, V, delayed rectifier activation, n, and cytosolic free Ca^{2+} concentration, c, are as follows:

$$\frac{dV}{dt} = -[I_{Ca} + I_K + I_{K(Ca)} + I_{K(ATP)}]/C_m \tag{1}$$

$$\frac{dn}{dt} = [n_\infty(V) - n]/\tau_n \tag{2}$$

$$\frac{dc}{dt} = f_{cyt} J_{mem}, \tag{3}$$

where C_m is the membrane capacitance, τ_n is the activation time constant for the delayed rectifier channel, $n_\infty(V)$ is the steady state function for the activation variable n, and J_{mem} is the Ca^{2+} flux through the plasma membrane. Since c represents the free Ca^{2+} concentration, we multiply J_{mem} by the fraction of free to total Ca^{2+}, f_{cyt}.

Expressions for the ionic currents are as follows:

$$I_{Ca} = g_{Ca} m_\infty(V)(V - V_{Ca}) \tag{4}$$

$$I_K = g_K n(V - V_K) \tag{5}$$

$$I_{K(Ca)} = g_{K(Ca)} \omega(V - V_K) \tag{6}$$

$$I_{K(ATP)} = g_{K(ATP)}(V - V_K). \tag{7}$$

Table 1. Parameter values for the basic model.

Parameter	Value	Parameter	Value
g_{Ca}	1200 pS	g_K	3000 pS
$g_{K(Ca)}$	300 pS	$g_{K(ATP)}$	230 pS
V_{Ca}	25 mV	V_K	−75 mV
C_m	5300 fF	α	4.5×10^{-6} fA^{-1} μM ms^{-1}
τ_n	16 ms	f_{cyt}	0.01
k_{PMCA}	0.2 ms^{-1}	K_D	0.3 μM
v_n	−16 mV	s_n	5 mV
v_m	−20 mV	s_m	12 mV

The conductance values and reversal potentials, along with other parameters, are listed in Table 1. The steady state activation functions have an increasing dependence on voltage and saturate at positive voltages:

$$m_\infty(V) = [1 + e^{(v_m - V)/s_m}]^{-1} \tag{8}$$

$$n_\infty(V) = [1 + e^{(v_n - V)/s_n}]^{-1}. \tag{9}$$

Since the gating of the Ca^{2+} channel is much faster than the gating of the K^+ channels, we assume rapid equilibrium and incorporate $m_\infty(V)$ directly into I_{Ca}. The variable ω is the fraction of K(Ca) channels activated by cytosolic Ca^{2+}:

$$\omega = \frac{c^5}{c^5 + k_D^5}, \tag{10}$$

where k_D is the dissociation constant for Ca^{2+} binding to the channel. The value of the exponent is not critical, other values could be used. Finally, the flux of Ca^{2+} through the membrane is

$$J_{mem} = -(\alpha I_{Ca} + k_{PMCA} c), \tag{11}$$

where α converts units of current to units of flux, and $k_{PMCA}c$ is the flux through the plasma membrane Ca^{2+} ATPase pumps.

2.2. ***Fast/slow analysis of bursting.*** The behavior of the basic model is shown in Fig. 1. Bursts of action potentials are generated on top of depolarized plateaus, followed by membrane hyperpolarization. The burst period is 2 s [Fig. 1(a)]. Action potentials are produced by the interaction of the 'fast' currents I_{Ca} and I_K, while the slow rhythm that packages impulses into bursts is generated by oscillations in $I_{K(Ca)}$. During the active spiking phase the cytosolic Ca^{2+} concentration rises [Fig. 1(b)], increasing the fraction of activated K(Ca) channels ω (not shown), thus increasing the K(Ca) conductance [Fig. 1(c)]. Since $I_{K(Ca)}$ is a hyperpolarizing

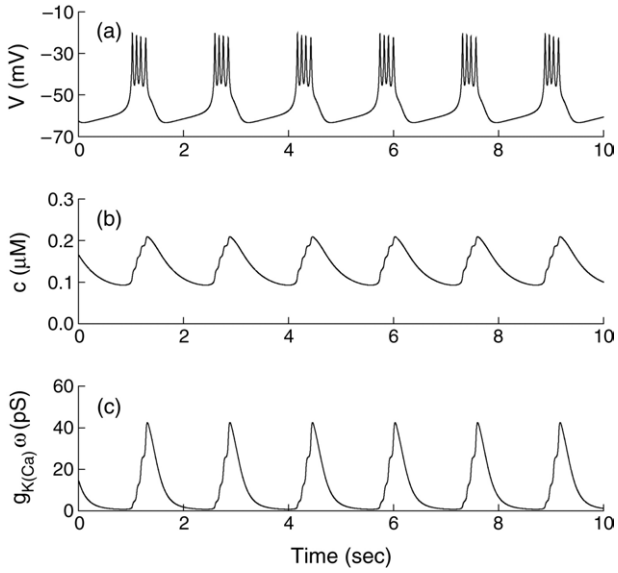

Figure 1. Bursting generated by the basic model, with $g_{K(Ca)} = 300$ pS. (a) Impulses ride on plateaus, with burst period of 2 s. (b) Cytosolic Ca^{2+} concentration rises during active phases and falls during silent phases. (c) The activity-dependent oscillations in c produce oscillations in the conductance of the K(Ca) channel, driving the bursting.

current, when $g_{K(Ca)}$ rises to a sufficiently high level the spiking terminates and the cell enters the hyperpolarized silent phase. During this phase c declines due to pumping of Ca^{2+} out of the cell, so the K(Ca) conductance declines. Eventually $I_{K(Ca)}$ is small enough to allow the cell to re-enter the spiking phase, and the cycle begins anew.

Another way to view the dynamics of bursting is through a fast/slow analysis (Rinzel, 1985), treating the slow variable, c, as a parameter of the subsystem of fast variables (V and n). A bifurcation digram for this fast subsystem is shown in Fig. 2 with ω [equation (10)] as the bifurcation parameter. The variable c could be used as the bifurcation parameter, but the dynamics are clearer with ω because total K(Ca) conductance is linear in ω. The bifurcation diagram and trajectories were generated with the program XPPAUT (Ermentrout, 2002).

For large values of ω the fast subsystem is at rest at a hyperpolarized voltage. These stable rest states make up the bottom branch of the z-shaped slow manifold ('z-curve') in Fig. 2. The lower branch turns and becomes unstable at a saddle node bifurcation, and then turns again at another saddle node bifurcation. The stationary branch regains stability for ω near 0 at a Hopf bifurcation. The branch of periodic solutions emerging from the Hopf bifurcation represents action potentials (both minimum and maximum V are indicated). It terminates at an infinite-period homoclinic bifurcation.

We now think of ω not as a parameter, but as a function of the slowly changing variable c, and superimpose on the bifurcation diagram the c nullcline, transformed

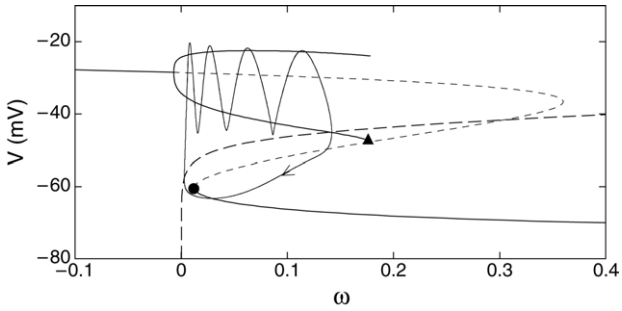

Figure 2. Fast/slow analysis of bursting with the basic model. Heavy solid curves represent stable branches, the light dashed curve represents an unstable branch, and the heavy dashed curve represents the c nullcline transformed according to equation (10) (the 'ω nullcline'). The lower saddle node bifurcation (circle) terminates the silent phase of bursting and the homoclinic bifurcation (triangle) terminates the periodic spiking branch. The burst trajectory is superimposed.

according to equation (10). We refer to this as the 'ω nullcline'. Below the ω nullcline the trajectory moves to the left, and above the nullcline it moves to the right. The superimposed burst trajectory follows along the bottom branch of the z-curve during the silent phase and along the periodic branch during the active phase. The spike rate is reduced as the trajectory approaches the homoclinic orbit at the end of the periodic branch, and the active phase ends when the trajectory falls below the middle branch of the z-curve.

If the nullcline does not intersect either the periodic branch or the bottom stationary branch, then bursting is produced. In the limit as the speed of the slow variable goes to zero, there is a transition from bursting to continuous spiking when the nullcline intersects the periodic branch (Terman, 1992). Here, however, c is not very slow, so the intersection must occur deeper into the periodic branch for the transition to occur.

With this basic model, the burst period depends on two things: the speed of the single slow variable c, and the distance that c (or ω) travels as it cycles between active and silent phases. The speed of c can be adjusted with the parameter f_{cyt}; reducing f_{cyt} to 0.0005 reduces the speed of c and increases the burst period to nearly 20 s, 10 times greater than with $f_{\text{cyt}} = 0.01$. With this reduction in the fraction of free Ca^{2+}, the slower time course of c has a sawtooth appearance. During the active phase c slowly rises and during the silent phase it slowly falls (Fig. 3). The Chay–Keizer model (Chay and Keizer, 1983) predicted such a sawtooth timecourse, but subsequent fluorescence recordings showed that Ca^{2+} typically rises quickly and equilibrates early in the active phase (Santos *et al.*, 1991). Thus, although reducing the speed of c succeeds in converting fast bursting to medium bursting, the resulting c timecourse is at odds with the experimental data.

The second mechanism for increasing the burst period is to increase the interval of bistability, that is, the horizontal distance between the lower saddle node

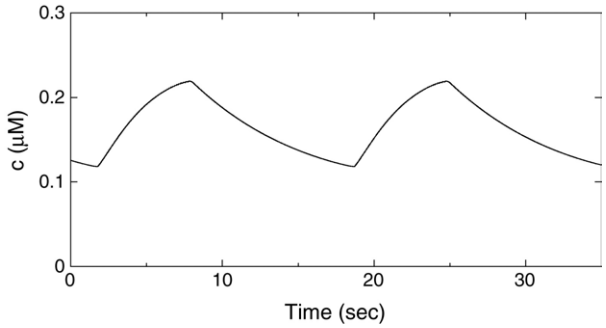

Figure 3. The burst period is increased when the fraction of free Ca^{2+}, f_{cyt}, is decreased to $f_{cyt} = 0.0005$. This results in a slow sawtooth Ca^{2+} oscillation, which is at odds with Ca^{2+} fluorescence data.

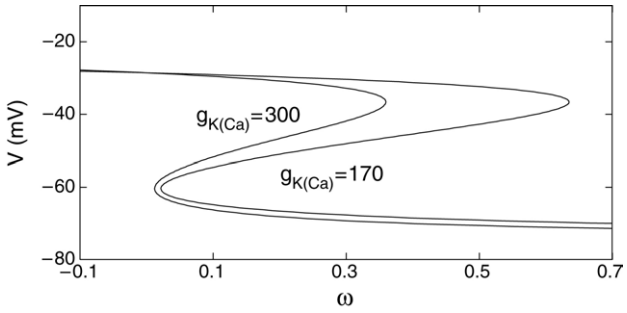

Figure 4. Decreasing the conductance of the K(Ca) current stretches the z-curve, resulting in a longer burst period. Only the stationary branches are shown.

bifurcation and the homoclinic bifurcation in Fig. 2. This can be done by reducing the conductance parameter $g_{K(Ca)}$, which stretches the z-curve (Fig. 4). However, the increase in burst period achieved through stretching is very limited, since if the z-curve is stretched too much the nullcline intersects the periodic branch and the model cell spikes continuously. For example, the bursting produced with $g_{K(Ca)} = 170$ pS has a period of 3 s, 50% greater than with $g_{K(Ca)} = 300$ pS. If $g_{K(Ca)}$ is decreased further to 160 pS the cell spikes continuously. It is difficult to attain anything near the 10-fold increase in burst period required to convert a fast burster into a medium burster. An alternative way to increase burst period while preserving the fast equilibration of c is given in the next section.

3. Bursting Model with Two Slow Variables

3.1. ***Roles of the endoplasmic reticulum.*** The ER acts as a high-capacity store for Ca^{2+} (Clapham, 1995). Ca^{2+} enters the ER via ATP-driven pumps in the ER membrane (SERCA pumps) and leaves through a leakage pathway and through inositol 1,4,5-trisphosphate receptor-channels, IP_3R (Berridge and Irvine, 1989). Thus, the ER acts as both a Ca^{2+} source and a Ca^{2+} sink.

The ER influences the electrical activity of many excitable cell types. In the β-cell, the ER is a target for several hormones and neurotransmitters. The parasympathetic transmitter acetylcholine (ACh) binds to muscarinic receptors in the β-cell membrane (Santos and Rojas, 1989) and activates phospholipase C, which produces IP_3 and diacylglycerol. The IP_3 activates IP_3R in the ER membrane, increasing the Ca^{2+} efflux from the ER (Berridge and Irvine, 1989). Application of ACh to mouse islets in the presence of glucose converts medium bursting to fast bursting with a depolarized silent phase (Gilon and Henquin, 2001). These changes result in enhanced insulin secretion, which is critical to the *in vivo* response after a meal (Woods and Porte, 1974).

Below we show how the ER acts as a filter to mold the kinetics of cytosolic Ca^{2+}. In Section 3.3 we demonstrate that oscillations in the ER Ca^{2+} concentration can be important in driving medium bursting, with the ER Ca^{2+} concentration playing the role of s_2 in the phantom bursting mechanism (Bertram *et al*., 2000). In Section 3.4 we show that the model can also account for the effects of muscarinic agonists.

3.2. ***Ca^{2+} concentration in the ER.*** We assume that the Ca^{2+} influx into the ER via SERCA pumps depends linearly on the cytosolic Ca^{2+} concentration:

$$J_{\text{SERCA}} = k_{\text{SERCA}} c. \tag{12}$$

The linear expressions for flux through SERCA and membrane pumps [equations (11) and (12)] are used for convenience in analysis. In particular, the c nullcline can then be calculated analytically. The results are similar if the standard non-linear expressions are used for both pumps.

The efflux out of the ER has two components. The Ca^{2+} leak is taken to be proportional to the gradient between Ca^{2+} concentrations in the cytosol and the ER (c_{er}):

$$J_{\text{leak}} = p_{\text{leak}}(c_{\text{er}} - c). \tag{13}$$

Ca^{2+} efflux through the IP_3R is the second component. We use a model based on Li and Rinzel (1994):

$$J_{\text{IP}_3} = O_\infty (c_{\text{er}} - c), \tag{14}$$

where O_∞ is the fraction of open channels. IP_3 channels are activated by IP_3 and by cytosolic Ca^{2+}, and are also inactivated by cytosolic Ca^{2+}. We assume that all three processes equilibrate rapidly, and use the following steady-state function in equation (14):

$$O_\infty = \left(\frac{c}{d_{\text{act}} + c}\right)^3 \left(\frac{\text{IP}_3}{d_{\text{IP}_3} + \text{IP}_3}\right)^3 \left(\frac{d_{\text{inact}}}{d_{\text{inact}} + c}\right)^3, \tag{15}$$

where the first factor represents activation by c, the second activation by IP_3, and the third inactivation by higher concentrations of c. For simplicity, we use IP_3 without brackets to represent the IP_3 concentration.

Table 2. Parameter values for model with ER.

Parameter	Value	Parameter	Value
k_{PMCA}	0.2 ms^{-1}	f_{er}	0.01
k_{SERCA}	0.4 ms^{-1}	p_{leak}	0.0005 ms^{-1}
d_{act}	0.35 μM	d_{IP_3}	0.5 μM
d_{inact}	0.4 μM	$V_{\text{cyt}}/V_{\text{er}}$	5

The net Ca^{2+} efflux from the ER is

$$J_{\text{er}} = J_{\text{leak}} + J_{\text{IP}_3} - J_{\text{SERCA}}. \tag{16}$$

Since this represents an additional influx term to the cytosolic Ca^{2+} compartment, we modify the differential equation for c:

$$\frac{dc}{dt} = f_{\text{cyt}}(J_{\text{mem}} + J_{\text{er}}). \tag{17}$$

For the ER Ca^{2+} concentration, J_{er} must be scaled by the ratio of the volumes of the cytoplasmic compartment (V_{cyt}) and the ER compartment (V_{er}):

$$\frac{dc_{\text{er}}}{dt} = -f_{\text{er}}(V_{\text{cyt}}/V_{\text{er}})J_{\text{er}}, \tag{18}$$

where f_{er} is the fraction of free Ca^{2+} in the ER.

In summary, the differential equations for the β-cell model with ER are given by equations (1), (2), (17) and (18). Parameter values are as given in Table 1, except those listed in Table 2. The IP_3 concentration is 0 unless stated otherwise.

3.3. ***Medium bursting via the phantom bursting mechanism.*** The ER Ca^{2+} concentration, like the cytosolic concentration, is a slow variable, albeit much slower. However, while c affects the membrane potential directly through K(Ca) conductance, c_{er} affects the membrane only indirectly through c. Geometrically, c_{er} modulates the c or ω nullcline, but has no effect on the z-curve. We therefore analyze the dynamics of the system through a fast/slow analysis as before, with ω as the bifurcation parameter. However, the nullcline now slowly changes as the ER fills and empties.

The c nullcline (with $IP_3 = 0$) is given by

$$c_\infty = \frac{p_{\text{leak}}c_{\text{er}} - \alpha I_{\text{Ca}}}{k_{\text{PMCA}} + p_{\text{leak}} + k_{\text{SERCA}}}, \tag{19}$$

which is then transformed by equation (10) to yield the ω nullcline. Fig. 5 shows the ω nullcline in the ω–V plane for several values of c_{er}. When c_{er} is increased, the nullcline is stretched, which has the effect of shifting it downward.

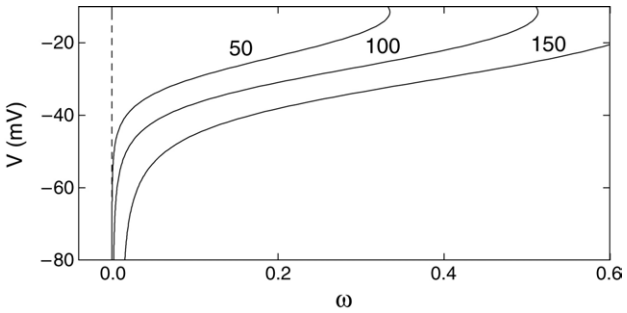

Figure 5. The ω nullcline for three values of the ER Ca^{2+} concentration (in μM). Increasing c_{er} stretches and lowers the nullcline.

As discussed earlier, one way to change the burst period is to stretch/compress the z-curve by decreasing/increasing the K(Ca) conductance (Fig. 4). With large conductance ($g_{K(Ca)} = 900$ pS) the z-curve is compressed and the β-cell model with ER generates a fast bursting oscillation (Fig. 6). Over the duration of a burst c_{er} varies from 100 to 101 μM, a small range which has little effect on the ω nullcline. One way to demonstrate the effects of the dynamics of c_{er} on bursting is to clamp c_{er} at its mean value. When c_{er} is clamped at 100.5 μM, the fast bursting oscillation persists. Thus, with a large K(Ca) conductance, the behavior of the enhanced model with two slow variables is very much like the behavior of the basic single-slow variable model (Fig. 1). Using the phase plane view, the dynamics can be described as in Fig. 2, except that there are tiny oscillations in the nullcline (not shown).

When the K(Ca) conductance is reduced ($g_{K(Ca)} = 700$ pS) the z-curve is stretched and the burst period is increased. As discussed earlier, with the single-slow variable model significant stretching produces continuous spiking since the phase point becomes stuck on the periodic branch. With the two-slow variable model, the z-curve can be stretched to a much greater extent and still produce bursting. This is because when the nullcline intersects the periodic branch the spiking activity increases the ER Ca^{2+} concentration, which slowly stretches and lowers the nullcline. Eventually the nullcline is lowered sufficiently so that the phase point escapes from the periodic branch and is attracted to the stationary bottom branch of the z-curve (Fig. 7, $c_{er} = 108$ μM). The phase point traverses most of the stationary branch before stalling again at the intersection with the nullcline. However, the cessation of spiking eliminates Ca^{2+} influx into the cell and into the ER, so there is a net reduction in c_{er} as Ca^{2+} continues to leak out of the ER. This results in a leftward shift of the ω nullcline, slowly moving the pseudo-equilibrium leftward along the stationary branch toward the saddle-node bifurcation. When this bifurcation is reached the phase point escapes from the stationary branch and is attracted to the periodic branch, restarting the active phase of bursting (Fig. 7, $c_{er} = 94$ μM).

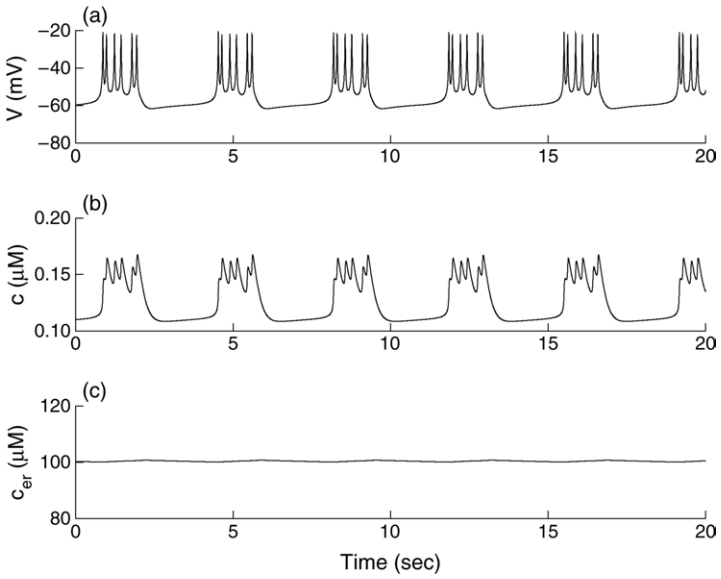

Figure 6. Fast bursting is produced when K(Ca) conductance is large, compressing the z-curve. The small c_{er} oscillations have little effect on the bursting. Parameter values are listed in Tables 1 and 2, except $g_{K(Ca)} = 900$ pS and $g_{K(ATP)} = 227.5$ pS.

This scenario results in a bursting oscillation (Fig. 8) with period an order of magnitude greater than that of fast bursting. Oscillations in both c and c_{er} are required: if c_{er} is clamped the cell either spikes continuously or is in a rest state. Thus, both slow variables are essential, and the burst period depends on the timescales of both variables. If the stretching is not extreme [$g_{K(Ca)}$ not too small], the trajectory only briefly stalls at the end of the active and silent phases, so most of the time is spent traversing the periodic and stationary branches and the c timescale dominates. If the stretching is extreme, the phase point stalls during most of the burst period, and the period is determined primarily by the c_{er} timescale. Slow bursting with a period of up to several minutes can be obtained by further reducing $g_{K(Ca)}$, which further stretches the z-curve (not shown).

The oscillations in c_{er} also result in a new qualitative feature of the c timecourse, the slowly decaying tail of c during the silent phase as the ER gives back the Ca^{2+} that it has taken up during the active phase [Fig. 8(b)]. There is also necessarily a slow rise of c during the active phase due to increased efflux of Ca^{2+} from the ER as it slowly fills. This rise is obscured by the rapid oscillations of c in Fig. 8(b), but it is essential as it is the only source of enhanced negative feedback that distinguishes the end of the active phase from the beginning. The mixture of fast and slow components in c, stemming from the intrinsic kinetics of c and from the ER, respectively, is a critical step toward bringing the c timecourse into agreement with the experimentally observed patterns. Further refinements will be achieved below by adding a second very slow process to the model (see Fig. 13).

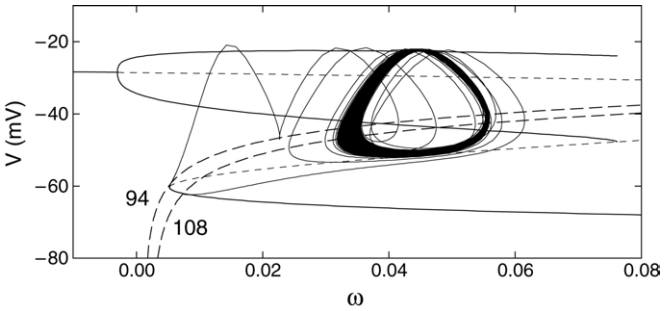

Figure 7. When the K(Ca) conductance is reduced to $g_{K(Ca)} = 700$ pS (with $g_{K(ATP)} = 230$ pS) the z-curve is stretched. As a result, the phase point stalls in both the active and silent phases, escaping only when activity-dependent changes in c_{er} (labelled) shifts the nullcline sufficiently far to the right or left.

3.4. ***Muscarinic fast bursting.*** In addition to glucose, pancreatic islets are controlled by the hypothalamus via the autonomic nervous system (Woods and Porte, 1974). Acetylcholine released from parasympathetic nerves enhances insulin secretion, and *in vitro* studies show that this is due partly to its effect on the islet electrical activity and Ca^{2+} dynamics (Gilon and Henquin, 2001). Acetylcholine binds to muscarinic receptors in the β-cell membrane, leading to the intracellular production of IP_3 and diacylglycerol (Santos and Rojas, 1989). IP_3 activates Ca^{2+} flux through the IP_3R [equation (14)], which increases cytosolic Ca^{2+} and enhances insulin secretion. DAG sensitizes the secretory machinery to Ca^{2+} (Bozem and Henquin, 1988), but this effect is beyond the scope of the present model.

Fig. 9 shows the effects of IP_3 on a medium bursting model cell (with parameter values as in Fig. 8). After 100 s the IP_3 concentration is increased from 0 to 0.3 μM. The immediate effect is a spike in the cytosolic Ca^{2+} concentration as Ca^{2+} floods out of the ER and into the cytosol. This hyperpolarizes the membrane through activation of $I_{K(Ca)}$. After the Ca^{2+} spike is dissipated by Ca^{2+} pumps in the plasma membrane, the cell again begins to burst. However, this bursting is much faster than the bursting prior to the addition of ACh (inset to panel A shows expanded view). This is because the rise in IP_3 and subsequent reduction in c_{er} changes the shape of the ω nullcline, so that it now intersects the z-curve in the same way as it did during the fast bursting described earlier. Fig. 10 shows the z-curve with ω nullcline prior to (dotted) and following (dashed) the addition of IP_3 (and after the transient hyperpolarization). The superimposed muscarinic burst trajectory does not stall in either the active or silent phase, and the bursting is driven entirely by ω. Indeed, when c_{er} is clamped at its average value of 53.1 μM the fast muscarinic bursting persists (not shown).

Although the transient hyperpolarization and increased burst frequency are consistent with experimental data (Gilon and Henquin, 2001), the simulation and the data differ in one respect. In most experimental recordings the silent phase of

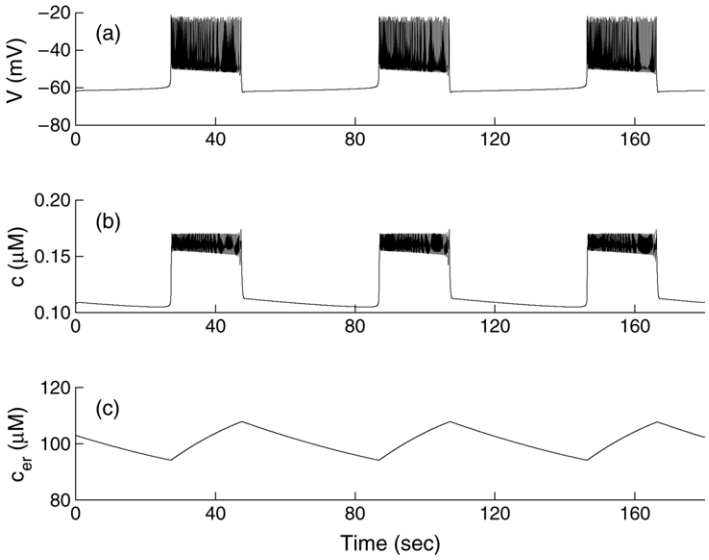

Figure 8. Medium bursting produced through the phantom bursting mechanism (with $g_{K(Ca)} = 700$ pS, $g_{K(ATP)} = 230$ pS). This requires activity-dependent oscillations in both c and c_{er}.

the muscarinic bursting is depolarized, while in the simulation the minimum silent phase voltage during muscarinic bursting is the same as that during medium bursting [Fig. 9(a)]. The depolarization is reflected in an elevated mean Ca^{2+} concentration, which is also not reproduced by the model [Fig. 9(b)].

The extra depolarization can be introduced into the model in at least two ways: (1) assume that the muscarinic agonist itself activates a depolarizing current, a receptor operated current (ROC) or (2) assume that depletion of the ER Ca^{2+} activates a store operated current (SOC). There is evidence for both in islets (Miura *et al*., 1996, 1997; Roe *et al*., 1998; Mears and Zimliki, 2003). Here we illustrate direct activation of a ROC by ACh,

$$I_{ACh} = g_{ACh}(V - V_{ACh}), \tag{20}$$

where $V_{ACh} = 0$.

Fig. 11 shows the effect of a muscarinic agonist when I_{ACh} is included in the model [equation (1)]. To simulate application of a muscarinic agonist, the IP_3 concentration is set to 0.3 μM and the ACh current conductance g_{ACh} is set to 15 pS. The extra depolarization provided by I_{ACh} elevates the silent phase voltage of the muscarinic bursting [Fig. 11(a)]. In terms of the phase plane analysis, this occurs for two reasons. One is that I_{ACh} lifts the bottom stationary branch of the z-curve. (Note that I_{ACh} is larger in magnitude at lower voltages.) The other reason is that the bursting is so fast that the phase point never actually reaches the bottom branch during the silent phase, but instead moves along a trajectory

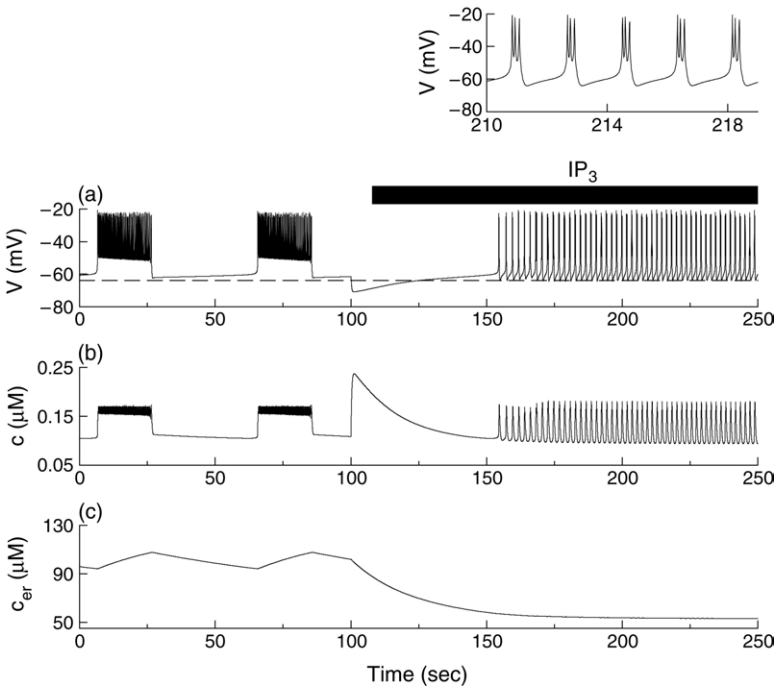

Figure 9. Conversion from medium bursting ($g_{K(Ca)} = 700$ pS, $g_{K(ATP)} = 230$ pS) to fast bursting produced by activation of IP_3 receptors/channels ($IP_3 = 0.3\ \mu$M as indicated). (a) Upon IP_3 application the membrane is initially hyperpolarized by $I_{K(Ca)}$, but then recovers into a fast bursting pattern (inset shows expanded view). The minimum silent phase voltage is not elevated following IP_3 application (dashed line). (b) Although the Ca^{2+} profile is changed, the mean concentration is unaffected by the IP_3. (c) The ER is largely drained by activation of IP_3 channels.

that lies between the middle and bottom branches, similar to the trajectory presented in Fig. 2. As a result of the elevated voltage, the mean Ca^{2+} concentration is also elevated [Fig. 11(b)], as observed in the experimental data (Bertram *et al.*, 1995).

We note that adding ROC alone, without dumping the stores, is sufficient to produce faster, depolarized bursting. However, while this is a theoretical possibility, it appears that β-cells do not work this way—muscarinic agonists do dump the stores. The point of the analysis in this section is that they must activate an inward current as well.

4. Bursting Model with Three Slow Variables

4.1. ***Evidence for nucleotide oscillations.*** Glucose metabolism provides the ATP that powers pumps, which maintain ionic gradients, and drives exocytosis. β-cells are unusual in that the nucleotide ratio, ADP/ATP, varies with the glucose

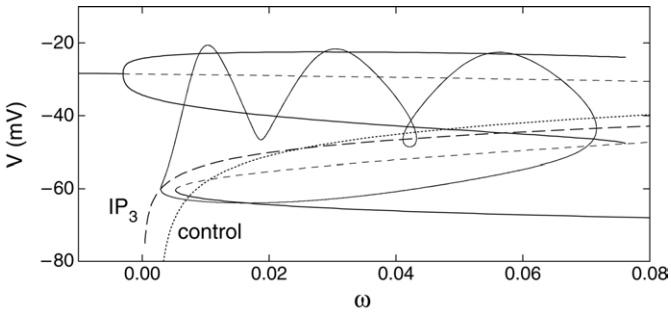

Figure 10. With $IP_3 = 0.3$ μM the shape of the ω nullcline is changed, so that the superimposed muscarinic bursting is driven entirely by ω. The dotted curve is the nullcline with $IP_3 = 0$ (and with $c_{er} = 108$ μM). The dashed curve is the nullcline with $IP_3 = 0.3$ (and with $c_{er} = 53$ μM). This latter nullcline was computed numerically, since equation (19) does not apply when $IP_3 \neq 0$. In both cases $g_{K(Ca)} = 700$ pS and $g_{K(ATP)} = 230$ pS.

concentration. At low glucose, the ratio is large, while at higher glucose levels the increased metabolism raises ATP relative to ADP, decreasing the nucleotide ratio. Through the nucleotide ratio glucose directly modulates β-cell electrical activity by controlling the activity of the nucleotide-sensitive current, $I_{K(ATP)}$ [equation (7); Ashcroft *et al*., 1984]. The conductance of the K(ATP) channel, $g_{K(ATP)}$, is large when the nucleotide ratio is large. Thus, when glucose is low, $g_{K(ATP)}$ is high, and β-cells are hyperpolarized. When the glucose concentration is elevated $g_{K(ATP)}$ is reduced and bursting is possible.

In the models described thus far $g_{K(ATP)}$ is constant, set at a low value to simulate the case of a stimulatory glucose level. There is, however, substantial evidence from mouse islets that the ADP/ATP ratio, the K(ATP) conductance, and oxygen consumption, an indicator of ATP production, are oscillatory even when the bath glucose concentration is constant (Dryselius *et al*., 1994; Larsson *et al*., 1996; Nilsson *et al*., 1996; Ainscow and Rutter, 2002; Kennedy *et al*., 2002). Most of the data support the hypothesis that oscillations in ADP/ATP are due to the influence of Ca^{2+} on ATP production or utilization (Ainscow and Rutter, 2002; Kennedy *et al*., 2002). Nucleotide oscillations may also result from oscillations in glycolysis (Longo *et al*., 1991; Nilsson *et al*., 1996; Tornheim, 1997), but in what follows we assume a Ca^{2+}-dependent pathway.

One possible mechanism for negative feedback of Ca^{2+} on ATP production in islets was postulated by Keizer and Magnus (Keizer and Magnus, 1989; Magnus and Keizer, 1997). These authors argued that Ca^{2+} reduces the mitochondrial membrane potential, thus reducing ATP production and increasing the ADP/ATP ratio. Evidence for this effect has recently been reported in mouse β-cells (Krippeit-Drews *et al*., 2000). An alternative mechanism for a Ca^{2+}-mediated increase in ADP/ATP is that Ca^{2+} pumps in the plasma membrane and in the ER membrane work harder when the cytosolic Ca^{2+} level is elevated. Since these pumps are powered by ATP hydrolysis, the level of ADP increases at the expense of ATP (Detimary *et al*., 1998).

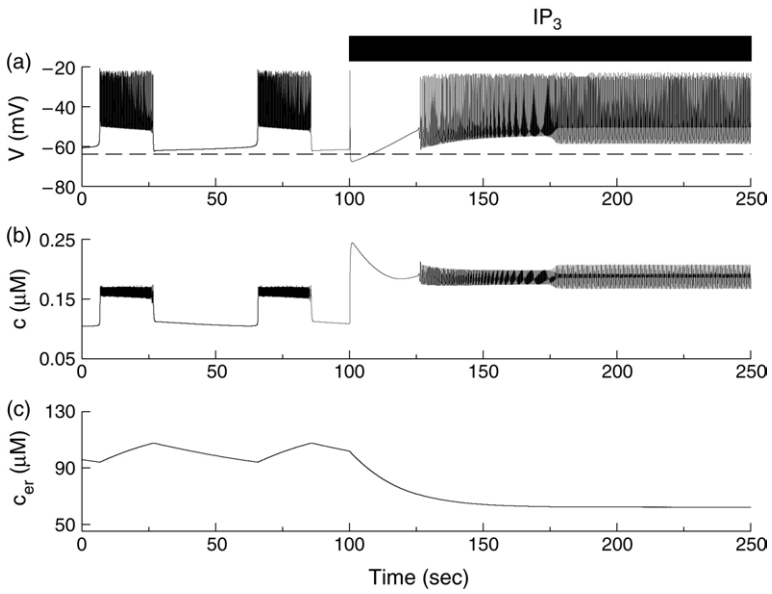

Figure 11. Conversion from medium bursting ($g_{K(Ca)} = 700$ pS, $g_{K(ATP)} = 230$ pS) to fast bursting ($IP_3 = 0.3\ \mu$M) when a depolarizing ACh current is included in the model ($g_{ACh} = 15$ pS). (a) The muscarinic bursting is now fast and the silent phase is depolarized above that of the prior medium bursting (dashed line). (b) The depolarized muscarinic bursting raises the average Ca^{2+} concentration. (c) The ER is drained by activation of IP_3 channels.

We assume that the nucleotide ratio $a = \text{ADP}/\text{ATP}$ satisfies the first-order kinetic equation

$$\frac{da}{dt} = (a_\infty(c) - a)/\tau_a. \tag{21}$$

The equilibrium function, $a_\infty(c)$, has an increasing sigmoidal dependence on cytosolic Ca^{2+} concentration:

$$a_\infty(c) = [1 + e^{(r-c)/s_a}]^{-1}. \tag{22}$$

This relation reflects either the inhibitory action of Ca^{2+} on mitochondrial membrane potential, or the increased utilization of ATP when Ca^{2+} concentration is elevated. The time constant, τ_a, is set to 5 min, consistent with data showing that nucleotide oscillations often occur on a timescale of several minutes. Finally, the hyperpolarizing K(ATP) current [equation (7)] is replaced by

$$I_{K(ATP)} = \overline{g}_{K(ATP)} a (V - V_K). \tag{23}$$

Parameter values are given in Table 3.

This simple model of the Ca^{2+}-dependent dynamics of the nucleotide ratio is meant to be qualitative in nature, capturing phenomenological features of the interaction rather than detailed quantitative or mechanistic aspects. A mechanistic

Table 3. Parameter values for model with nucleotide dynamics.

Parameter	Value	Parameter	Value
r	0.14 μM	s_a	0.1 μM
τ_a	300 000 ms	$\overline{g}_{K(ATP)}$	500 pS

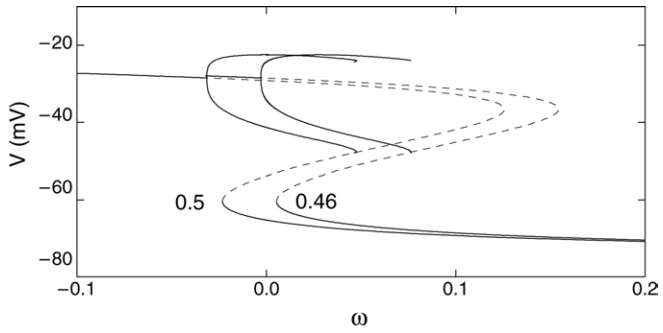

Figure 12. The z-curve for two values of the nucleotide ratio a. Increasing the ratio translates the z-curve to the left.

model of the negative feedback of Ca^{2+} on ATP production has been developed previously (Keizer and Magnus, 1989; Magnus and Keizer, 1997), and our results carry over to a model that includes this more detailed Keizer–Magnus formulation.

4.2. ***Slow bursting via metabolic oscillations.*** The nucleotide ratio a enters into the system through the V equation [equation (1)], so it affects the z-curve in the fast subsystem bifurcation diagram. The conductance of $I_{K(ATP)}$ is larger for larger values of a, so less ω is needed to give the same amount of inhibition through $I_{K(Ca)}$. Thus, increasing a translates the z-curve to the left (Fig. 12). Inclusion of the a dynamics exploits a geometrical degree of freedom unused up to this point, which complements the motions of the ω nullcline described previously.

Because a adjusts slowly to changes in c (τ_a is large), it oscillates over a very narrow range of values during fast bursting and the effect on the z-curve is negligible. When $g_{K(Ca)}$ is reduced to 700 pS, a value that produced medium bursting when K(ATP) conductance was constant (Fig. 8), the system still produces medium bursting (not shown). Now a varies between 0.460 and 0.464, and the effect on the z-curve is small, but no longer negligible. If a is held fixed at 0.462, near its average value, the bursting slows down, with a longer active phase and a longer silent phase.

The real impact of a dynamic nucleotide ratio, however, is seen when $g_{K(Ca)}$ is reduced further, to 100 pS (Fig. 13). This stretches the z-curve so much that c_{er}-induced motion of the nullcline is insufficient to liberate the phase point from its stalled state. If the nucleotide ratio is held constant, the system either spikes continuously or remains in a hyperpolarized rest state, depending on the value of a.

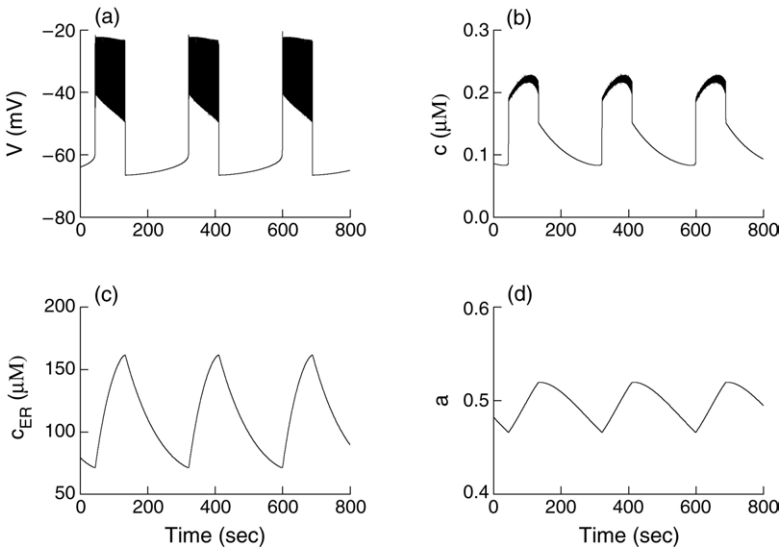

Figure 13. Slow bursting produced when the z-curve is stretched by reducing $g_{K(Ca)} = 100$ pS. All three slow variables, c, c_{er}, and a, interact to produce this oscillation, but the rate-limiting variable is a.

When the z-curve is stretched to this extent, oscillations in a [Fig. 13(d)] are required to shift the z-curve sufficiently far to the left to permit the phase point to escape the active phase, and sufficiently far to the right to permit the phase point to escape the silent phase. Because of the large time constant τ_a, however, these z-curve translations are very slow. As a result, the bursting that occurs can have a period of up to several minutes [Fig. 13(a)]. With $g_{K(Ca)} = 100$ pS the burst period is 275 s, within the range of periods often observed in β-cells and islets (Ashcroft *et al.*, 1984; Valdeolmillos *et al.*, 1996; Liu *et al.*, 1998; Zhang *et al.*, 2003). The ER Ca^{2+} concentration now varies over a wide range of values during a burst [Fig. 13(c)], which results in large shifts in the ω nullcline during a burst. However, the slow changes in a are rate limiting and are essential for the slowest bursting rhythms.

The prolonged bursts increase the amplitude of the c_{er} oscillations, which enhances the slow tail of c during the silent phase. [Fig. 13(b); compare with the c time-course in the model with ER but constant nucleotide ratio, Fig. 8(b).] The slow rise of c during the active phase is initially also enhanced but is subsequently blunted by the rise in a, which reduces spike frequency and hinders Ca^{2+} entry. Although experimentally these features have not been explored systematically, impressionistic evidence suggests that slow tails are seen most prominently during the slowest bursting, and that slow rises are seen only rarely (Zhang *et al.*, 2003).

4.3. ***Slow bursting persists when Ca^{2+} stores are depleted.*** Two key experimental findings shed light on the role of the ER and the nucleotide ratio in β-cell

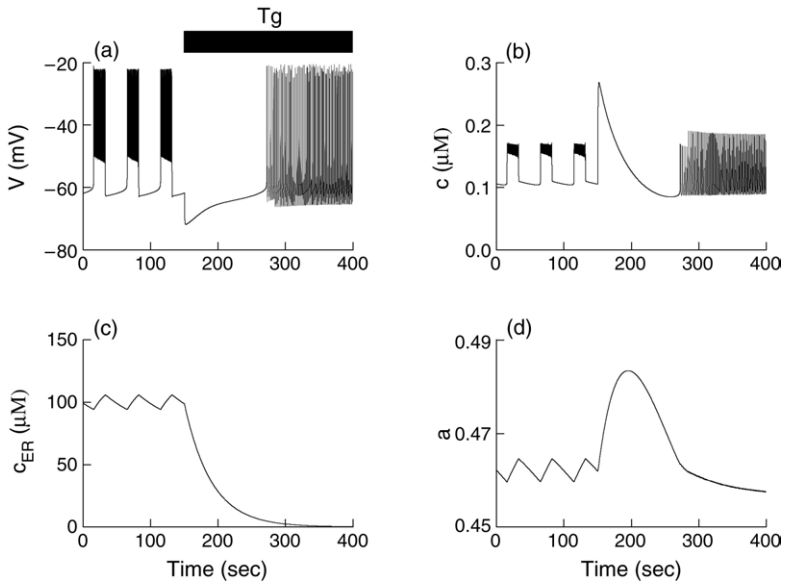

Figure 14. Simulated application of the SERCA pump blocker thapsigargin ($k_{\mathrm{SERCA}} = 0$) converts medium bursting [$g_{\mathrm{K(Ca)}} = 700$ pS] to fast bursting.

bursting. First, it has been shown that islets exhibiting a medium bursting rhythm convert to continuous spiking when SERCA pumps are inhibited by thapsigargin (Worley III *et al*., 1994) or thapsigargin plus acetylcholine (Bertram *et al*., 1995). Second, it has been shown that β-cells exhibiting a slow oscillation in free cytosolic Ca^{2+} (presumably due to slow bursting) continue to oscillate with a higher, but still low, frequency following application of thapsigargin (Liu *et al*., 1995, 1998; Miura *et al*., 1997; Gilon *et al*., 1999). These data raise the question of how the ER can have such a dramatic impact on medium bursting, while having little effect on slow bursting. We address this here by simulating the application of thapsigargin (Tg) to medium and slow bursting model cells. This is done by setting the SERCA pump rate k_{SERCA} to 0.

When Tg is applied to a model cell exhibiting medium bursting [$g_{\mathrm{K(Ca)}} = 700$ pS], the rhythm is converted to a fast bursting pattern (Fig. 14). This is due to the precipitous drop in the ER Ca^{2+} concentration in response to SERCA pump blockage, which affects the ω nullcline in two ways: (1) it is now sharper, so it intersects the z-curve only on the middle (unstable) branch, and (2) it is now virtually static. It is the middle-branch intersection that allows for the fast bursting driven entirely by c, just as in the case of muscarinic bursting (Figs. 9 and 10). This pattern does not quite match the experimental data, which indicates continuous spiking in the presence of Tg (Worley III *et al*., 1994). If the ER is assumed to activate a depolarizing SOC current, then simulated application of Tg does elicit a continuous spiking pattern. However, then ACh also converts medium bursting to continuous spiking rather than fast bursting.

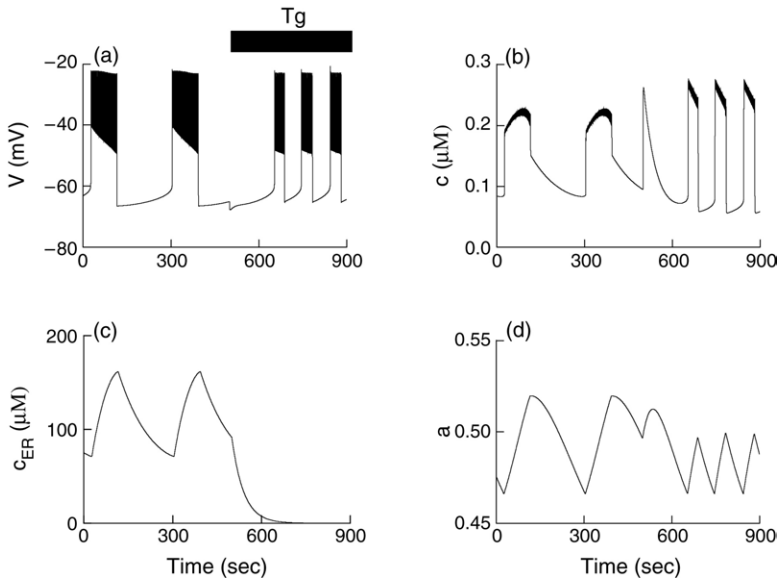

Figure 15. (a) Slow bursting [$g_{K(Ca)} = 100$ pS] persists when SERCA pumps are blocked ($k_{SERCA} = 0$). (b) The cytoslic Ca^{2+} rises to a higher level and has no Ca^{2+} tail following Tg application. (c) The ER drains following Tg application. (d) The slow bursting is driven by oscillations in both c_{er} and the nucleotide ratio before Tg application, but solely by the nucleotide ratio after Tg application.

When application of Tg is simulated in a slow bursting cell [$g_{K(Ca)} = 100$ pS] the response is quite different. Rather than the dramatic increase in burst frequency, the slow bursting persists, though with an increase in frequency (Fig. 15), as seen in the experiments cited above. In the model, this works because the slow bursting is driven primarily by nucleotide oscillations. When the SERCA pumps are blocked and the ER is drained [Fig. 15(c)], the ω nullcline again changes shape and becomes static. In the slow bursters, however, the z-curve is stretched more because $g_{K(Ca)}$ is small, so the ω nullcline intersects the bottom stationary branch as well as the periodic branch. The bursting is thus driven purely by a slow movement of the z-curve without help from movement of the ω nullcline. The shorter period is due to the different shape of the nullcline, which is now sharper.

When the SERCA pumps are inhibited, the timecourse of c also has a different shape. Most notably, the slow Ca^{2+} tail during the silent phase, described in Section 4.2, disappears in Tg because the ER can no longer sequester Ca^{2+}. Also, the cytosolic Ca^{2+} declines throughout the active phase in Tg because the growing inhibitory effect of a on Ca^{2+} entry is not balanced by the slow rise in c normally produced by ER filling. Finally, c rises to a much higher level in Tg. All of these features match the experimental data when SERCA is blocked pharmacologically (Gilon *et al.*, 1999; Arredouani *et al.*, 2002a) or when a component of SERCA is knocked out genetically (Arredouani *et al.*, 2002b).

5. Effects of K(ATP) Channel Modulators

5.1. ***Triphasic response to glucose.*** Islets respond to step increases in the extracellular glucose concentration with a triphasic pattern of insulin secretion, consisting of an initial delay, followed by a rapid peak of insulin release, followed by a lower level of sustained, oscillatory secretion (Grodsky, 1989). A triphasic pattern in islet electrical activity is also observed (Meissner and Atwater, 1976). Upon application of glucose the islet remains hyperpolarized for a minute or more, followed by a period of continuous spiking, followed by sustained bursting. (If the glucose concentration is very large, more than 20 mM, the islet spikes continuously and never enters a bursting mode.) The triphasic response to glucose is finally also exhibited in the cytosolic Ca^{2+} concentration (Roe *et al*., 1993), which initially declines upon glucose application (phase 0). This is followed by an elevation that lasts for more than a minute (phase 1), and finally by sustained oscillations (phase 2). In this section we show that the model with ER and nucleotide dynamics can account for these complex transients.

There is considerable evidence that the initial decline in the Ca^{2+} concentration is due to upregulation of SERCA pumps, initiated by the increased production of ATP concentration when glucose is elevated (Roe *et al*., 1994; Chow *et al*., 1995; Gilon *et al*., 1999). The electrical spiking, rise in Ca^{2+} concentration, and increased insulin secretion that characterize phases 1 and 2 are mainly due to the closure of K(ATP) channels in response to the decreased ADP/ATP ratio (Ashcroft *et al*., 1984).

In the model, we simulate the low glucose state by reducing the SERCA pump rate to $k_{\text{SERCA}} = 0.05\ \text{ms}^{-1}$ and increasing the equilibrium ADP/ATP ratio by decreasing the parameter r to 0 [equation (22)]. With these parameter values the model cell goes to a hyperpolarized rest state with low cytosolic and ER Ca^{2+} concentrations (Fig. 16). Because of the low value of r, the resting value of a is relatively large. In the phase plane, the ω nullcline intersects the z-curve on the bottom branch, far to the right of the lower saddle node bifurcation (not shown).

Glucose application is simulated by stepping k_{SERCA} and r to their default values, $k_{\text{SERCA}} = 0.4\ \text{ms}^{-1}$ and $r = 0.14\ \mu\text{M}$ (Fig. 16, horizontal bar). In response to the increase in r, a slowly declines. In the phase plane, this slowly shifts the z-curve to the right. However, the ω nullcline continues to intersect the bottom stationary branch of the z-curve while a declines, and the system remains hyperpolarized. Thus, the initial response to glucose is a delay while the z-curve slowly shifts to the right. In addition, since k_{SERCA} is increased, enough pumping of cytosolic Ca^{2+} from the cytosol to the ER occurs to cause a noticeable drop in the cytosolic Ca^{2+} concentration [Fig. 16(b)]. Thus, both the delay and the Ca^{2+} drop characteristic of phase 0 in experiments are captured by the model.

Within three minutes of the simulated application of glucose, the nucleotide ratio [and thus the K(ATP) conductance] have fallen to a level sufficiently low that the system begins to spike. In the phase plane, the z-curve has shifted far enough to

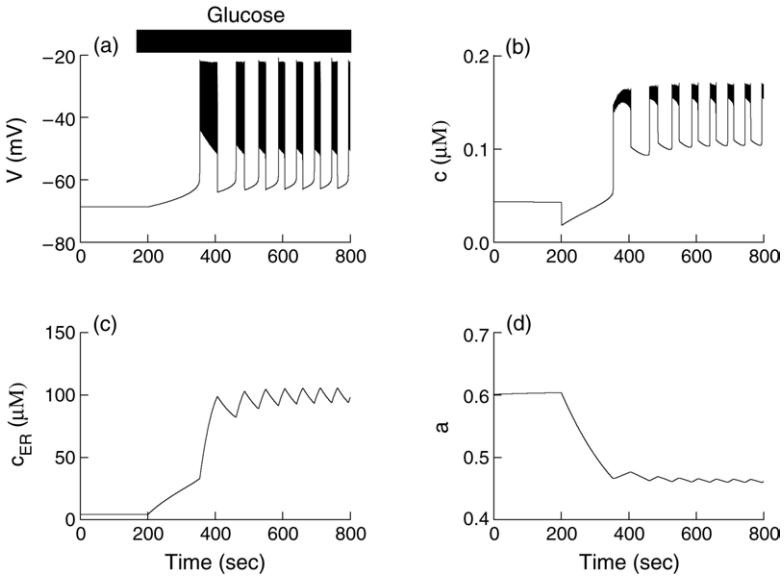

Figure 16. Triphasic response to glucose. The initial low glucose state is simulated by setting $k_{\mathrm{SERCA}} = 0.05\ \mathrm{ms}^{-1}$ and $r = 0$. Stimulatory glucose is simulated by increasing both parameters, to $k_{\mathrm{SERCA}} = 0.4\ \mathrm{ms}^{-1}$ and $r = 0.14\ \mu$M. Throughout the simulation $g_{\mathrm{K(Ca)}} = 700$ pS and $\bar{g}_{\mathrm{K(ATP)}} = 500$ pS.

the right that the nullcline has passed the lower saddle-node and now intersects the periodic branch. The prior hyperpolarization has left the ER largely depleted, in spite of the modest refilling during phase 0, and this prevents the nullcline from reaching the homoclinic termination of the periodic branch until the ER fills to the level it normally attains during phase 2 [Fig. 16(c)]. Thus, the phase 1 response of extended spiking activity is a prolonged active phase caused by the delayed filling of the ER. Phase 2 commences when the ER is filled.

A prediction of this model is that there should be little or no phase 1 in slowly bursting cells or islets. This is in fact what was found in Zhang *et al*. (2003), where both medium and slow islets were observed. The duration of the first burst was about the same in both medium and slow islets, but the ratio of the second burst duration to the first burst duration approached 1 for the slower islets.

5.2. ***Slow bursting in tolbutamide and thapsigargin.*** If, as we postulate, the ER Ca^{2+} and nucleotide oscillations are key players in medium and slow bursting, then the bursting may be greatly altered if one of these variables is perturbed. Such was the case when the SERCA pump blocker thapsigargin was applied to β-cells and islets. However, as we described earlier, Tg had a large effect on medium bursting, but not slow bursting, which we attribute to the presence of an oscillatory K(ATP) conductance. A natural experiment, then, is to pharmacologically alter both the ER Ca^{2+} and the K(ATP) conductance. This experiment has recently been performed (Fridlyand *et al*., 2003a). First, the K(ATP) channel blocker tolbutamide was added

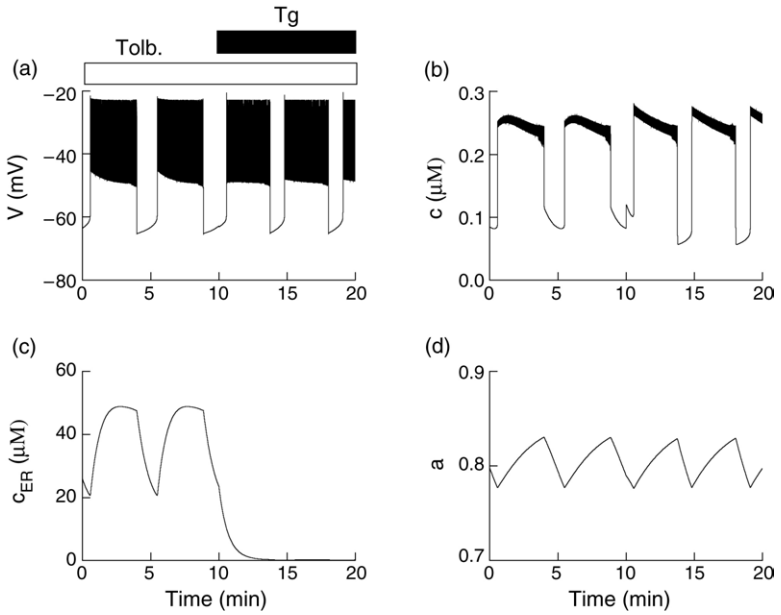

Figure 17. Slow bursting produced by simulated application of tolbutamide (Tolb., $\bar{g}_{K(ATP)} = 300$ pS) in the presence of a low glucose concentration ($k_{SERCA} = 0.1$ ms^{-1}, $r = 0.04$ μM). Application of thapsigargin (Tg, $k_{SERCA} = 0$) is simulated after 10 min. Bursting is driven by c_{er} and a prior to Tg application, and by a following Tg application. Throughout the simulation, $g_{K(Ca)} = 100$ pS.

to a bath containing a low (3 mM) glucose concentration. This resulted in a slow bursting oscillation that persisted when Tg was added to the bath. Here we interpret the results of this experiment with our mathematical model.

To simulate a low (but non-zero) glucose concentration, we reduce the SERCA pump rate to $k_{SERCA} = 0.1$ ms^{-1}, and increase the equilibrium nucleotide ratio by setting $r = 0.04$ μM. With the default value of K(ATP) conductance, $\bar{g}_{K(ATP)} = 500$ pS, the system comes to rest at a hyperpolarized voltage, as in experiments. Application of tolbutamide reduces the availability of K(ATP) channels, which we simulate by reducing $\bar{g}_{K(ATP)}$ to 300 pS. With the reduction of this hyperpolarizing conductance, the model cell becomes electrically active. In fact, with the small value of $g_{K(Ca)}$ chosen here, it exhibits a slow bursting pattern (Fig. 17). One might expect the system to spike continuously, since much of the conductance for the current ($I_{K(ATP)}$) that normally drives slow bursting has been removed by tolbutamide. Nonetheless, the system bursts because the nucleotide ratio is able to compensate for the reduction in $\bar{g}_{K(ATP)}$, by moving to a higher mean value [compare Fig. 17(d) to Fig. 13(d)]. Thus, although $\bar{g}_{K(ATP)}$ has been reduced, the actual conductance of the current, $\bar{g}_{K(ATP)}a$, is in an appropriate range for slow bursting driven primarily by a. For the same reason, when the application of Tg is simulated ($k_{SERCA} = 0$), the slow bursting persists, with a slight increase in frequency (Fig. 17).

This scenario requires that the nucleotide ratio be able to adapt to K(ATP) block and to oscillate, driving the slow bursting. It is also important that tolbutamide does not block all K(ATP) channels, or that elevations in ADP/ATP are able to open some channels that had been blocked by tolbutamide. Indeed, one experimental study found that islets repolarized, presumably due to the opening of K(ATP) channels, when ATP production was inhibited by NaN_3 in the presence of 50 μM tolbutamide (Henquin, 1998). Thus, either not all K(ATP) channels are blocked by this concentration of tolbutamide, or those that are blocked can be opened by lowering the ATP concentration (and increasing ADP/ATP). However, if too much tolbutamide is applied, bursting may convert to continuous spiking (Miura *et al*., 1997). The model would agree with this, because a cannot rise sufficiently to overcome the reduction in $g_{K(ATP)}$. Finally, it has been observed that it is not possible (or very difficult) to obtain bursting with tolbutamide alone—a minimum amount of glucose is required (Cook and Ikeuchi, 1989; Henquin, 1998). The model would agree with this also, because a cannot oscillate if r is too small.

6. DISCUSSION

Our starting point for this study was the Chay–Keizer model for β-cell electrical activity. That model successfully explained a number of key experimental observations, but the predicted approximately mono-exponential rise and fall of cytosolic Ca^{2+} concentration, c (Fig. 1), proved to be incorrect. Further, lacking an internal Ca^{2+} store (ER), Chay–Keizer was unable to address phenomena related to store dumping. Here, we have developed step-by-step a more comprehensive model that accounts for a much wider range of phenomena.

We have not included all known or hypothesized β-cell mechanisms, but only the minimum modifications needed to explain the data. By keeping the models simple, we have been able to show how three slow processes, cytosolic Ca^{2+}, ER Ca^{2+}, and the nucleotide ratio ADP/ATP, articulate geometrically as well as biophysically. We have also established a unified theoretical framework in which to analyze a diverse family of models. All the mechanisms included here have been incorporated into models previously, but the combination, the tuning to reproduce a wide spectrum of phenomena, and the analysis are novel.

The first extension to Chay–Keizer described here was to add the ER (we will call this the ER model, for brevity). The key role of the ER is to slow the rise and fall of c, rendering c, and hence $g_{K(Ca)}$, slow enough to drive medium and slow bursting; without the ER only fast bursting is possible (Fig. 1). When Ca^{2+} influx is suddenly increased, as at the beginning of the active phase of a burst, c rises rapidly [Fig. 8(b)]. The elevation in c causes the ER to fill slowly, which increases the rate of diffusive efflux [equation (13)]. This leads to a slow rise in c, which remains in quasisteady state with c_{er}. During the silent phase, the process is reversed: c undergoes an initial rapid drop followed by a slow decline. Thus,

Table 4. Summary of models.

Slow variables	All burst periods	ACh	Tg	Triphasic	Tolbutamide plus Tg
c (1)	No	No	No	No	No
c, c_{er} (6) and (8)	Yes	Yes (9) and (11)	No	No	No
c, c_{er}, a (13)	Yes	Yes	Yes (14) and (15)	Yes (16)	Yes (17)

c now has two components, a fast component from its own intrinsic kinetics and a slow component imparted by the ER. This eliminates most of the error in the c kinetics of the unmodified Chay–Keizer model.

The two components of c also function like the slow variables s_1 and s_2 in the generic phantom bursting model (Bertram *et al*., 2000). If the initial fast rise in c during the active phase of a burst activates sufficient $g_{K(Ca)}$ to terminate spiking, fast bursting ensues (Fig. 6). If not, the balance of the required negative feedback develops on the slow ER timescale to produce medium (Fig. 8) or slow bursting.

The core element of the ER model, slow negative feedback by c_{er}, which indirectly activates $g_{K(Ca)}$, was already contained in the last models of Chay (1996, 1997). This mechanism was also discovered independently in a non-β-cell model by Shorten and Wall (2000). Chay's model was able to reproduce the wide range of β-cell oscillation periods through variation of the ER efflux rate. In contrast to the 'phantom' effects of changing $g_{K(Ca)}$, which stretches the z-curve (Fig. 4), p_{leak} affects the time constant and operating range of c_{er}. Geometrically, it controls the speed at which the c nullcline sweeps back and forth across the z-curve in the v–c phase plane.

In both our ER model and Chay's, dumping the ER, whether by increasing efflux or blocking influx, increases burst frequency, in agreement with experiment. In order to obtain the observed depolarization as well, one must assume that an additional inward current is activated, either by the agonist (ROC; Fig. 11) or by the store depletion itself (SOC). While we can simulate all the observed behaviors, we cannot yet do it with one consistent set of parameters for both IP_3R activation and SERCA inhibition. It remains to be seen whether these discrepancies reflect fundamental shortcomings in the model or repairable quantitative deficiencies.

Thus, adding an ER to Chay–Keizer largely corrects the kinetics of c and accounts for ER perturbations (due to ACh or Tg), and also vastly extends the range of oscillation periods. These points are summarized in Table 4. However, the ER model still fails to account for the observation that slow bursting is insensitive to store depletion (Miura *et al*., 1997; Liu *et al*., 1998). We remedied this by adding $g_{K(ATP)}$ as a second negative feedback target for Ca^{2+}. (We will call this the ER-ATP model, for brevity.) Unlike the response of $g_{K(Ca)}$ to Ca^{2+}, the response of metabolism to Ca^{2+} was assumed to have intrinsically slow kinetics that are even slower than c_{er}. Consequently, slow bursting occurs (preferentially) when $g_{K(Ca)}$ is

small, and can persist when the stores are dumped by thapsigargin (Fig. 15). In contrast, $g_{K(Ca)}$ and c_{er} are still important for medium bursting, which is vulnerable to SERCA blockade (Fig. 14).

Another recent model (Fridlyand *et al*., 2003b) offers an alternative explanation for the persistence of slow bursting in thapsigargin. In that model, medium bursting is driven mainly by fluctuations in c_{er} via SOC, and hence is sensitive to SERCA blockers. Slow bursting occurs when the ER is relatively depleted and SOC is saturated. This allows a second slower negative feedback process to develop, activation of the electrogenic Na^+–K^+ pump by accumulation of intracellular Na^+. Although the latter depends indirectly on intracellular Ca^{2+} through the Na^+–Ca^{2+} exchanger, it is apparently relatively insensitive to the state of the ER. Thus, as in our ER-ATP model, the presence of a second slow process that is essentially independent of the ER protects slow oscillations from ER perturbations. In both models, the c timecourse is modified when Tg is applied in agreement with experimental observations [Fig. 15(b)].

Fridlyand *et al*. (2003a) have shown that slow bursting persists if both SERCA and $g_{K(ATP)}$ are blocked, suggesting that neither c_{er} nor $g_{K(ATP)}$ is essential for slow oscillations. We have shown here, however (Fig. 17), that slow oscillations in the ER-ATP model can persist in the presence of both thapsigargin and tolbutamide provided sufficient residual $g_{K(ATP)}$ remains. Nonetheless, if slow oscillations can in fact occur with both SERCA and $g_{K(ATP)}$ completely blocked, our model would have to be revised.

The ER-ATP model can also reproduce for the first time the key elements of the triphasic response to a step in glucose from basal to stimulatory levels (Fig. 16). Phase 0 is due to a slow decline in a, while phase 1 is due to the slow filling of the ER. The mechanism of phase 1 differs from a previous model of ours (Bertram *et al*., 1995). Although phase 1 was also mediated by slow filling of the ER in the older model, the enhanced firing was due to activation of SOC rather than a blunting of Ca^{2+}-dependent negative feedback.

Another key difference in Bertram *et al*. (1995) was that c_{er} was much slower than in the current model. Therefore, c_{er} did not vary significantly during phase 2 bursting, and c exhibited only its fast component. In such a model, with just two Ca^{2+} compartments, ER and cytosol, the ER can influence plasma membrane channels in two ways: Ca^{2+}-dependent channels, such as K(Ca), respond to fluxes of ER Ca^{2+}, and SOC responds to the level of ER Ca^{2+}. Therefore, when the ER is super-slow, it influences phase 2 bursting only by setting the level of SOC conductance. Further, even when the store is dumped by a rise in IP_3, there is only a transient increase in burst frequency while the store is equilibrating to its new, lower level, unless SOC is present. In the current model, in contrast, the ER is always sourcing or sinking Ca^{2+} and can influence firing rate continually without the need of SOC. The slow components of c seen experimentally during phase 2 suggest that the new model is closer to the truth. Thus, in this study we have demonstrated that a suitably configured ER can control phase 1, phase 2, and

muscarinic bursting largely through the effects of Ca^{2+} fluxes on $g_{K(Ca)}$, with SOC playing a secondary role.

In addition to limitations already mentioned, one obvious oversight in the current model is the experimental observation that thapsigargin blocks $g_{K(Ca)}$ (Goforth *et al*., 2002), whereas the current model erroneously predicts an *increase*. This can be fixed by adding a third Ca^{2+} compartment, a subspace between the ER and the plasma membrane. Qualitatively, that model can do everything the current model does, provided slow Ca^{2+}-dependent nucleotide dynamics are included, and much of the analysis presented here carries over.

The ability of each of the three models described in this paper, the Chay–Keizer model, the ER model, and the ER-ATP model, to reproduce experimental observations is summarized in Table 4. The first column of the table lists the model slow variables and figure numbers for the first instances in which the model was used. The second refers to the ability of the model to produce fast, medium, and slow bursting. The third refers to the effects of ACh, where medium bursting is converted to fast bursting. The fourth refers to the effects of Tg, both on slow bursting (remains slow) and on medium bursting (bursting speeds up or converts to continuous spiking). The fifth column refers to the triphasic response to glucose (initial delay, then continuous spiking, then bursting). The last column refers to the ability of the model to produce slow bursting in the presence of tolbutamide and thapsigargin. The figure number that illustrates each behavior is given in parentheses. Computer codes for each model and each simulated experimental manipulation (suitable for the XPPAUT software package) can be downloaded from http://mrb.niddk.nih.gov/sherman. Model animations are also included at this site, illustrating the dynamics of each model in the ω–V plane.

In conclusion, we end up with a model that is only a little more complicated than Chay–Keizer, but is more correct and can explain much more. The core is still negative feedback by cytosolic Ca^{2+}, now on two targets: $g_{K(Ca)}$, whose slow kinetics derive from the ER, and $g_{K(ATP)}$, whose slow kinetics may derive from metabolism. There is much that has been left out and much that the model still cannot do. Some phenomena requiring future effort include the effects of agonists that elevate *c*AMP, such as glucagon-like peptide and caffeine, and epinephrine, which inhibits insulin secretion and converts medium bursting to slow.

ACKNOWLEDGEMENTS

Much of the inspiration for this study came from the models of the late Theresa Chay. Ground work by former post-doc Gerda de Vries and of summer students Bernadette Baumeister and Tijan Watt was critical in extracting the key insights from those models. We also acknowledge analysis performed by Chip Zimliki in the course of his Ph. D. thesis work. Finally, we thank Camille Daniel for checking the equations in the manuscript and for writing computer codes for our distribution

web site. R. Bertram was supported by National Science Foundation grants DMS-9981822 and DMS-0311856.

REFERENCES

Ainscow, E. K. and G. A. Rutter (2002). Glucose-stimulated oscillations in free cytosolic ATP concentration imaged in single islet β-cells. *Diabetes* **51**, S162–S170.

Arredouani, A., J.-C. Henquin and P. Gilon (2002a). Contribution of the endoplasmic reticulum to the glucose-induced $[Ca^{2+}]_c$ response in mouse pancreatic islets. *Am. J. Physiol.* **1330**, E982–E991.

Arredouani, A. *et al*. (2002b). SERCA3 ablation does not impair insulin secretion but suggests distinct roles of different sarcoendoplasmic reticulum Ca^{2+} pumps for Ca^{2+} homeostasis in pancreatic β-cells. *Diabetes* **51**, 3245–3253.

Ashcroft, F. M., D. E. Harrison and S. J. H. Ashcroft (1984). Glucose induces closure of single potassium channels in isolated rat pancreatic β-cells. *Nature* **312**, 446–448.

Atwater, I., C. M. Dawson, A. Scott, G. Eddlestone and E. Rojas (1980). The nature of the oscillatory behavior in electrical activity for pancreatic β-cells, in *Biochemistry and Biophysics of the Pancreatic β-cell*, G. Thieme (Ed.), New York: Verlag, pp. 100–107.

Bergsten, P. (1995). Slow and fast oscillations of cytoplasmic Ca^{2+} in pancreatic islets correspond to pulsatile insulin release. *Am. J. Physiol.* **268**, E282–E287.

Bergsten, P., E. Grapengiesser, E. Gylfe, A. Tengholm and B. Hellman (1994). Synchronous oscillations of cytoplasmic Ca^{2+} and insulin release in glucose-stimulated pancreatic islets. *J. Biol. Chem.* **269**, 8749–8753.

Berridge, M. J. and R. F. Irvine (1989). Inositol phosphates and cell signalling. *Nature* **341**, 197–205.

Bertram, R., J. Previte, A. Sherman, T. A. Kinard and L. S. Satin (2000). The phantom burster model for pancreatic β-cells. *Biophys. J.* **79**, 2880–2892.

Bertram, R., P. Smolen, A. Sherman, D. Mears, I. Atwater, F. Martin and B. Soria (1995). A role for calcium release-activated current (CRAC) in cholinergic modulation of electrical activity in pancreatic β-cells. *Biophys. J.* **68**, 2323–2332.

Bordin, S., A. C. Boschero, E. M. Carneiro and I. Atwater (1995). Ionic mechanisms involved in the regulation of insulin secretion by muscarinic agonists. *J. Membrane Biol.* **148**, 177–184.

Bozem, M. and J. C. Henquin (1988). Glucose modulation of spike activity independently from changes in slow waves of membrane potential in mouse β-cells. *Pflügers Arch.* **413**, 147–152.

Chay, T. R. (1996). Electrical bursting and luminal calcium oscillation in excitable cell models. *Biol. Cybern.* **75**, 419–431.

Chay, T. R. (1997). Effects of extracellular calcium on electrical bursting and intracellular and luminal calcium oscillations in insulin secreting pancreatic β-cells. *Biophys. J.* **73**, 1673–1688.

Chay, T. R. and J. Keizer (1983). Minimal model for membrane oscillations in the pancreatic β-cell. *Biophys. J.* **42**, 181–190.

Chou, H.-F. and E. Ipp (1990). Pulsatile insulin secretion in isolated rat islets. *Diabetes* **39**, 112–117.

Chow, R. H., P.-E. Lund, S. Löser, U. Panten and E. Gylfe (1995). Coincidence of early glucose-induced depolarization with lowering of cytoplasmic Ca^{2+} in mouse pancreatic β-cells. *J. Physiol. (Lond.)* **485**, 607–617.

Clapham, D. E. (1995). Calcium signalling. *Cell* **80**, 259–268.

Cook, D. L., W. E. Crill and D. Porte Jr. (1981). Glucose and acetylcholine have different effects on the plateau pacemaker of pancreatic islet cells. *Diabetes* **30**, 558–561.

Cook, D. L. and M. Ikeuchi (1989). Tolbutamide as mimic of glucose on β-cell electrical activity: ATP-sensitive K^+ channels as common pathway for both stimuli. *Diabetes* **38**, 416–421.

Cook, D. L. and E. Perara (1982). Islet electrical pacemaker response to alpha-adrenergic stimulation. *Diabetes* **31**, 985–990.

Dean, P. M. and E. K. Mathews (1970). Glucose-induced electrical activity in pancreatic islet cells. *J. Physiol. (Lond.)* **210**, 255–264.

Detimary, P., P. Gilon and J.-C. Henquin (1998). Interplay between cytoplasmic Ca^{2+} and the ATP/ADP ratio: a feedback control mechanism in mouse pancreatic islets. *Biochem. J.* **333**, 269–274.

Dryselius, S., P.-E. Lund, E. Gylfe and B. Hellman (1994). Variations in ATP-sensitive K^+ channel activity provide evidence for inherent metabolic oscillations in pancreatic β-cells. *Biochem. Biophys. Res. Commun.* **205**, 880–885.

Ermentrout, G. B. (2002). *Simulating, Analyzing, and Animating Dynamical Systems: A Guide to XPPAUT for Researchers and Students*, Philadelphia: SIAM Books.

Fridlyand, L. E., N. Tamarina and L. H. Philipson (2003a). Role of Na^+ and signaling molecules in regulation of slow Ca^{2+} dynamics in pancreatic β-cells: a computational study. *Diabetes* **52**, A368.

Fridlyand, L. E., N. Tamarina and L. H. Philipson (2003b). Modeling of Ca^{2+} flux in pancreatic β-cells: role of the plasma membrane and intracellular stores. *Am. J. Physiol. (Endocrinol Metab)* **285**, E138–154.

Gilon, P., A. Arredouani, P. Gailly, J. Gromada and J.-C. Henquin (1999). Uptake and release of Ca^{2+} by the endoplasmic reticulum contribute to the oscillations of the cytosolic Ca^{2+} concentration triggered by Ca^{2+} influx in the electrically excitable pancreatic β-cell. *J. Biol. Chem.* **274**, 20197–20205.

Gilon, P. and J.-C. Henquin (2001). Mechanisms and physiological significance of the cholinergic control of pancreatic β-cell function. *Endocrine Rev.* **22**, 565–604.

Goforth, P. B., R. Bertram, F. A. Khan, M. Zhang, A. Sherman and L. S. Satin (2002). Calcium-activated K^+ channels of mouse β-cells are controlled by both store and cytoplasmic Ca^{2+}: experimental and theoretical studies. *J. Gen. Physiol.* **120**, 307–322.

Grodsky, G. M. (1989). A new phase of insulin secretion. How will it contribute to our understanding of β-cell function? *Diabetes* **38**, 673–678.

Henquin, J. C. (1998). A minimum of fuel is necessary for tolbutamide to mimic the effects of glucose on electrical activity in pancreatic β-cells. *Endocrinology* **139**, 993–998.

Keizer, J. and G. Magnus (1989). ATP-sensitive potassium channel and bursting in the pancreatic β cell. *Biophys. J.* **56**, 229–242.

Keizer, J. and P. Smolen (1991). Bursting electrical activity in pancreatic β cells caused by Ca^{2+}- and voltage-inactivated Ca^{2+} channels. *Proc. Natl. Acad. Sci. USA* **88**, 3897–3901.

Kennedy, R. T., L. M. Kauri, G. M. Dahlgren and S.-K. Jung (2002). Metabolic oscillations in β-cells. *Diabetes* **51**, S152–S161.

Kinard, T. A., G. de Vries, A. Sherman and L. S. Satin (1999). Modulation of the bursting properties of single mouse pancreatic β-cells by artificial conductances. *Biophys. J.* **76**, 1423–1435.

Krippeit-Drews, P., M. Dufer and G. Drews (2000). Parallel oscillations of intracellular calcium activity and mitochondrial membrane potential in mouse pancreatic β-cells. *Biochem. Biophys. Res. Commun.* **267**, 179–183.

Lang, D. A., D. R. Matthews, M. Burnett and R. C. Turner (1981). Brief, irregular oscillations of basal plasma insulin and glucose concentrations in diabetic man. *Diabetes* **30**, 435–439.

Larsson, O., H. Kindmark, R. Bränström, B. Fredholm and P.-O. Berggren (1996). Oscillations in K_{ATP} channel activity promote oscillations in cytoplasmic free Ca^{2+} concentration in the pancreatic β-cell. *Proc. Natl. Acad. Sci. USA* **93**, 5161–5165.

Li, Y.-X. and J. Rinzel (1994). Equations for $InsP_3$ receptor-mediated [Ca^{2+}] oscillations derived from a detailed kinetic model: a Hodgkin–Huxley like formalism. *J. Theor. Biol.* **166**, 461–473.

Liu, Y.-J., E. Grapengiesser, E. Gylfe and B. Hellman (1995). Glucose induces oscillations of cytoplasmic Ca^{2+}, Sr^{2+} and Ba^{2+} in pancreatic β-cells without participation of the thapsigargin-sensitive store. *Cell Calcium* **18**, 165–173.

Liu, Y.-J., A. Tengholm, E. Grapengiesser, B. Hellman and E. Gylfe (1998). Origin of slow and fast oscillations of Ca^{2+} in mouse pancreatic islets. *J. Physiol. (Lond.)* **508**, 471–481.

Longo, E. A., K. Tornheim, J. T. Deeney, B. A. Varnum, D. Tillotson, M. Prentki and B. E. Corkey (1991). Oscillations in cytosolic free Ca^{2+}, oxygen consumption, and insulin secretion in glucose-stimulated rat pancreatic islets. *J. Biol. Chem.* **266**, 9314–9319.

Magnus, G. and J. Keizer (1997). Minimal model of β-cell mitochondrial Ca^{2+} handling. *Am. J. Physiol.* **273**, C717–C733.

Martín, F. and B. Soria (1995). Amino acid-induced $[Ca^{2+}]_i$ oscillations in single mouse pancreatic islets. *J. Physiol. (Lond.)* **486**, 361–371.

Matthews, D. R., B. A. Naylor, R. G. Jones, G. M. Ward and R. C. Turner (1983). Pulsatile insulin secretion has greater hypoglycemic effect than continuous delivery. *Diabetes* **32**, 617–621.

Mears, D. and C. Zimliki (2003). Muscarinic agonists activate Ca^{2+} store-operated and -independent ionic currents in insulin-secreting HIT-T15 cells and mouse pancreatic β-cells. *J. Membrane Biol.* (in press).

Meissner, H. P. and I. J. Atwater (1976). The kinetics of electrical activity of beta cells in response to a square wave stimulation with glucose or glibenclamide. *Horm. Metab. Res.* **8**, 11–16.

Miura, Y., P. Gilon and J.-C. Henquin (1996). Muscarinic stimulation increases Na^+ entry in pancreatic B-cells by a mechanism other than the emptying of intracellular Ca^{2+} pools. *Biochem. Biophys. Res. Commun.* **224**, 67–73.

Miura, Y., J.-C. Henquin and P. Gilon (1997). Emptying of intracellular Ca^{2+} stores stimulates Ca^{2+} entry in mouse pancreatic β-cells by both direct and indirect mechanisms. *J. Physiol. (Lond.)* **503**, 387–398.

Nilsson, T., V. Schultz, P.-O. Berggren, B. E. Corkey and K. Tornheim (1996). Temporal patterns of changes in ATP/ADP ratio, glucose 6-phosphate and cytoplasmic free Ca^{2+} in glucose-stimulated pancreatic β-cells. *Biochem. J.* **314**, 91–94.

O'Meara, N. M., J. Sturis, J. D. Blackman, M. M. Byrne, J. B. Jaspan, J. R. Thistlethwaite and K. S. Polonsky (1993). Oscillatory insulin secretion after pancreas transplant. *Diabetes* **42**, 855–861.

Rinzel, J. (1985). Bursting oscillations in an excitable membrane model, in *Ordinary and Partial Differential Equations*, B. D. Sleeman and R. J. Jarvis (Eds), Lecture Notes in Mathematics **1151**, Berlin: Springer, pp. 304–316.

Roe, M. W., M. E. Lancaster, R. J. Mertz, J. F. Worley III and I. D. Dukes (1993). Voltage-dependent intracellular calcium release from mouse islets stimulated by glucose. *J. Biol. Chem.* **268**, 9953–9956.

Roe, M. W., L. H. Philipson, C. J. Frangakis, A. Kuznetsov, R. J. Mertz, M. E. Lancaster, B. Spencer, J. F. Worley III and I. D. Dukes (1994). Defective glucose-dependent endoplasmic reticulum Ca^{2+} sequestration in diabetic mouse islets of Langerhans. *J. Biol. Chem.* **269**, 18279–18282.

Roe, M. W., J. F. Worley III, F. Qian, N. Tamarina, A. A. Mittal, F. Dralyuk, N. T. Blair, R. J. Mertz, L. H. Philipson and I. D. Dukes (1998). Characterization of a Ca^{2+} release-activated nonselective cation current regulating membrane potential and $[Ca^{2+}]_i$ oscillations in transgenically derived β-cells. *J. Biol. Chem.* **273**, 10402–10410.

Sánchez-Andrés, J., A. Gomis and M. Valdeolmillos (1995). The electrical activity of mouse pancreatic β-cells recorded in vivo shows glucose-dependent oscillations. *J. Physiol. (Lond.)* **486**, 223–228.

Santos, R. M. and E. Rojas (1989). Muscarinic receptor modulation of glucose-induced electrical activity in mouse pancreatic B-cells. *FEBS Lett.* **249**, 411–417.

Santos, R. M., L. M. Rosario, A. Nadal, J. Garcia-Sancho, B. Soria and M. Valdeolmillos (1991). Widespread synchronous $[Ca^{2+}]_i$ oscillations due to bursting electrical activity in single pancreatic islets. *Pflügers Arch.* **418**, 417–422.

Shorten, P. R. and D. J. Wall (2000). A Hodgkin–Huxley model exhibiting bursting oscillations. *Bull. Math. Biol.* **62**, 695–715.

Smolen, P. and J. Keizer (1992). Slow voltage inactivation of Ca^{2+} currents and bursting mechanisms for the mouse pancreatic β-cell. *J. Membrane Biol.* **127**, 9–19.

Terman, D. (1992). The transition from bursting to continuous spiking in excitable membrane models. *J. Nonlinear Sci.* **2**, 135–182.

Tornheim, K. (1997). Are metabolic oscillations responsible for normal oscillatory secretion? *Diabetes* **46**, 1375–1380.

Valdeolmillos, M., A. Gomis and J. V. Sánchez-Andrés (1996). In vivo synchronous membrane potential oscillations in mouse pancreatic β-cells: lack of co-ordination between islets. *J. Physiol. (Lond.)* **493**, 9–18.

Woods, S. C. and D. Porte Jr. (1974). Neural control of the endocrine pancreas. *Physiol. Rev.* **54**, 596–619.

Worley, J. F. III, M. S. McIntyre, B. Spencer, R. J. Mertz, M. W. Roe and I. D. Dukes (1994). Endoplasmic reticulum calcium store regulates membrane potential in mouse islet β-cells. *J. Biol. Chem.* **269**, 14359–14362.

Zhang, M., P. Goforth, R. Bertram, A. Sherman and L. Satin (2003). The Ca^{2+} dynamics of isolated mouse β-cells and islets: implications for mathematical models. *Biophys. J.* **84**, 2852–2870.

Received 15 September 2003 and accepted 22 December 2003